ACS Photonics

Open Access

pubs.acs.org/journal/apchd5

Article

Single-Photon Level Dispersive Fourier Transform: Ultrasensitive Characterization of Noise-Driven Nonlinear Dynamics

Lynn Sader, Surajit Bose, Anahita Khodadad Kashi, Yassin Boussafa, Raktim Haldar, Romain Dauliat, Philippe Roy, Marc Fabert, Alessandro Tonello, Vincent Couderc, Michael Kues,* and Benjamin Wetzel*

Cite This: *ACS Photonics* 2023, 10, 3915−3928

Read Online

ACCESS | Metrics & More | Article Recommendations | Supporting Information

ABSTRACT: Dispersive Fourier transform is a characterization technique that allows directly extracting an optical spectrum from a time domain signal, thus providing access to real-time characterization of the signal spectrum. However, these techniques suffer from sensitivity and dynamic range limitations, hampering their use for special applications in, e.g., high-contrast characterizations and sensing. Here, we report on a novel approach to dispersive Fourier transform-based characterization using single-photon detectors. In particular, we experimentally develop this approach by leveraging mutual information analysis for signal processing and hold a performance comparison with standard dispersive Fourier transform detection and statistical tools. We apply the comparison to the analysis of noise-driven nonlinear dynamics arising from well-known modulation instability processes. We demonstrate that with this dispersive Fourier transform approach, mutual information metrics allow for successfully gaining insight into the fluctuations associated with modulation instability-induced spectral broadening, providing qualitatively similar signatures compared to ultrafast photodetector-based dispersive Fourier transform but with improved signal quality and spectral resolution (down to 53 pm). The technique presents an intrinsically unlimited dynamic range and is extremely sensitive, with a sensitivity reaching below the femtowatt (typically 4 orders of magnitude better than ultrafast dispersive Fourier transform detection). We show that this method can not only be implemented to gain insight into noise-driven (spontaneous) frequency conversion processes but also be leveraged to characterize incoherent dynamics seeded by weak coherent optical fields.

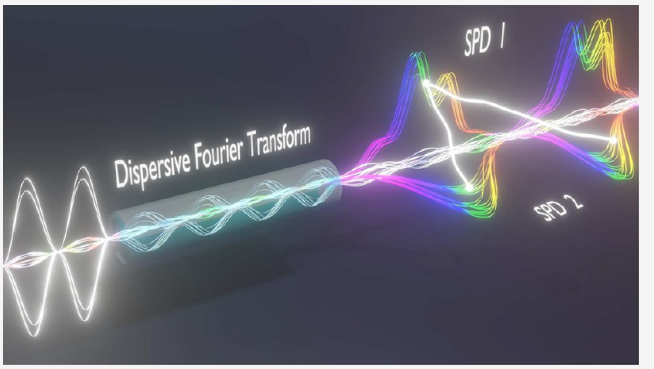

KEYWORDS: *nonlinear photonics, fiber optics, real-time characterization techniques, spectral correlation, modulation instability*

INTRODUCTION

Ultrafast and precise optical characterization techniques are the cornerstone of numerous achievements in physics, ranging from the detection of gravitational waves emitted by the merger of black holes[1] to the accurate measurements of subatomic particles and their subpicosecond oscillations.[2] Over the years, numerous advances in characterization techniques occurred and proved essential in the measurement of ultrashort pulses, associated with broadband spectral signals in the frequency domain. Techniques inherently based on dispersive time-stretch,[3−5] such as dispersive Fourier transform (DFT)[6,7] and time-lens (TL)[8,9] systems, proved successful for the characterization of incoherent processes requiring the measurement of ultrafast and non-repetitive events. Specifically, DFT transforms a broadband optical signal into a time-stretched waveform replica of the spectrum.[4,5] The analogous spectral waveform can thus be readily captured with a single-shot measurement of the temporal intensity profile.[4,10−12] DFT thus allows for the rapid acquisition and the subsequent analysis of large spectral data sets as required for the study of statistical outliers,[13,14] fast dynamical evolution,[15,16] or the implementation of machine learning in photonics.[17,18]

When dealing with optical signal monitoring, approaches such as direct spectrometry or pulse autocorrelation have now become mainstream as they can provide key information on optical signals.[19] Conversely, for advanced metrology, optical interferometry techniques have been developed to provide access to the complete ultrashort pulse properties in phase and intensity (FROG, X-FROG, etc.)[20] and eventually allow for single-shot characterization (SPIDER, GRENOUILLE, SPI-

Received: May 26, 2023
Published: October 25, 2023

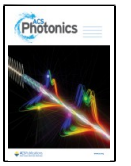

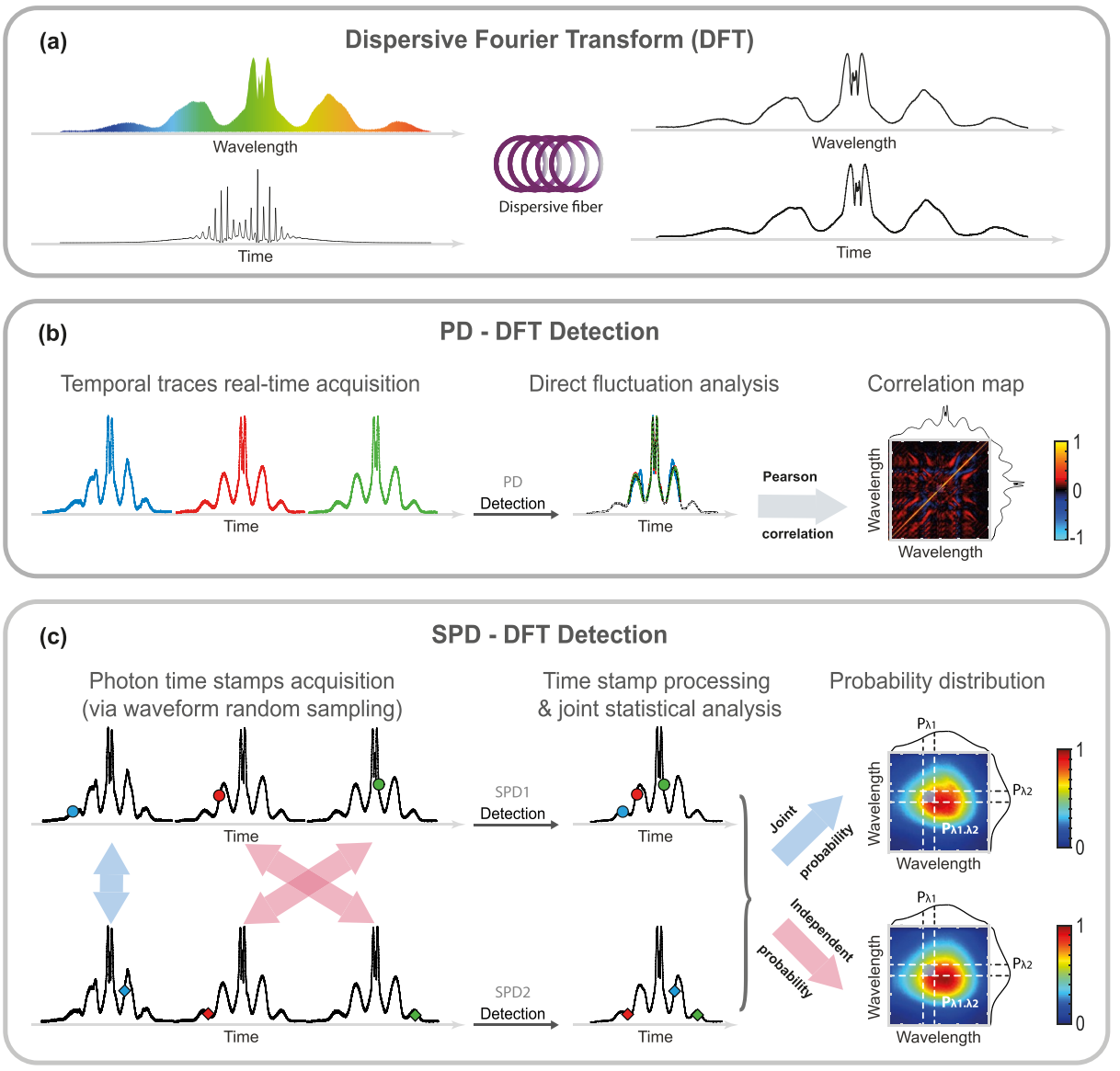

Figure 1. Schematic of DFT principle and associated detection schemes: (a) A broadband optical signal is transformed into a temporal waveform replica via a purely (linear) dispersive effect, allowing for real-time measurement of the fluctuating spectrum in the temporal domain. (b) Real-time DFT detection using a photodiode (PD) allows for sequential acquisition of the shot-to-shot spectra. These fluctuations can be statistically analyzed for the reconstruction of a spectral correlation map between the wavelengths of 2000 fluctuating spectra (Pearson correlation). (c) DFT detection using two single-photon detectors (SPDs) and statistical postprocessing of correlated photoevents (i.e., time-stamps) allows for discriminating intrapulse dynamics (blue arrows) and interpulse dynamics (red arrows). While visually similar, the analysis of joint and independent probabilities between the time-stamps of different photoevents can be leveraged to reconstruct a spectral map of mutual information analogous to Pearson correlation maps.

RIT, etc.).[21−24] These techniques are however limited regarding the specific properties of the signal to be measured (power, spectral coverage, bandwidth, etc.), and their operation may be complex in terms of optical alignment, pulse synchronization, or signal retrieval. For direct detection, optoelectronic characterization (via ultrafast photodetectors) is intrinsically bandwidth-limited and prevents the measurement of pulses in the picosecond regime (or below). In the frequency domain, typical optical spectrum analyzers (OSAs) rely on a long measurement time and can only provide averaged spectral measurements over multiple pulse periods. To overcome such constraints, dispersive time-stretch techniques enabling convenient access to single-shot, real-time, and ultrafast characterization in the spectral and temporal domains are now available.[6,7]

Real-time characterization techniques have been instrumental in gaining insights into fundamental aspects of photonics, nonlinear dynamics, chaotic systems, and complexity.[6,7,15,25,26] For instance, DFT techniques first allowed for the experimental study of incoherent frequency conversion processes, such as modulation instability (MI): The technique enabled the capture of nonrepetitive single-shot spectra with high-throughput (typically at MHz laser repetition rate), thus allowing the identification of extreme event formation, the statistical analysis of broadband spectral fluctuations, and the quantification of correlation features within complex noise-driven dynamics.[13,14,27−29] Moreover, when combining DFT

https://doi.org/10.1021/acsphotonics.3c00711
ACS Photonics 2023, 10, 3915−3928

with time-lens approaches, one can gain insight into the optical field build-up and evolution within a laser cavity.[16,30−34] Due to its simplicity and efficiency, DFT techniques have become a standard characterization tool, covering applications such as laser development, ultrafast microscopy, spectroscopy, or velocimetry.[35−38]

However, DFT faces several technical challenges: The spectral resolution is limited by the detection bandwidth of the photodiode or oscilloscope, which can reach a few tens of GHz. In this frequency range, photodiodes present limited sensitivity with poor noise figures while high-speed oscilloscopes, featured with 8−12 bits of digitalization, suffer from low dynamic ranges.[39] In this framework, one cannot achieve real-time spectral measurements with over 30 dB contrast as required for characterizing incoherent broadband pulses in demanding signal processing applications.[17,18,40] Several approaches have been demonstrated to circumvent these issues, which include loss compensation, advanced processing, and multipoint detector arrays.[18,36,38,41,42] Other potential improvements in DFT spectral resolution are expected from laser repetition rate decimation (via, e.g., pulse picking) along with significant dispersive time-stretch (using longer dispersive fibers of recirculating fiber loops) to avoid temporal signal overlap,[7] but they, in turn, strongly hamper the (instantaneous) signal intensity to be detected in the time domain. Overall, these DFT technique variations and mitigation schemes come at the expense of a decreased resolution or sensitivity, finally imposing a performance trade-off.

Recently, sparse temporal measurement techniques based on single-photon detection have proved successful in addressing sensitivity issues of ultrafast photodiodes. Indeed, single-photon detectors (SPD) have followed tremendous technological improvements and can reach extremely low timing jitter (down to a few picoseconds) while ensuring excellent sensitivity (quantum efficiency over 90%) and low instrumental noise (50 photons/s). This technological progress was instrumental in the development of highly resolved quantum measurements in the temporal and spectral domains[43−46] but also proved extremely relevant for applications in coherent signal processing[47] and imaging,[48,49] where quantum-inspired DFT measurements can play the role of ultrasensitive spectrometers.[50] However, when it comes to real-time (or shot-to-shot) monitoring of incoherent spectral dynamics, the sparse detection and random sampling of (at best) one photon per DFT spectrum with a unique single-photon detector drastically hamper the statistical analysis of broadband spectral fluctuations.

In this paper, we report on an innovative variation of standard DFT techniques, leveraging multiple single-photon detectors to provide better sensitivity, higher resolution, and an excellent dynamic range for demanding incoherent spectral characterization. Using a hybrid DFT scheme along with quantum-inspired correlation detection, we show that our approach is suitable for the analysis of complex nonlinear dynamics involving weak and incoherent processes. Specifically, we show that by studying the phenomena of MI, our technique is capable of providing a fine spectral correlation analysis between noise-driven and weakly driven multifrequency mixing processes. Compared to standard DFT measurement techniques, our approach yields similar qualitative signatures but with a finer spectral resolution and sensitivity enabling access to the onset of narrow linewidth and weak incoherent amplification processes out of reach of previous approaches. In this context, we demonstrate that such improved performances allow for the analysis of spectral instabilities with high resolution (as low as 53 pm), high sensitivity (below the femtowatt level), and a dynamic range expected to reach over 80 dB, thus illustrating the potential to shed light on noise-driven processes at the transition between quantum and nonlinear optics. Interestingly, the developed diagnostic tools provide distinctive features (e.g., sensitivity and dynamic range) that make them compatible with demanding machine learning strategies[17] and useful for tailoring nonlinear interactions in fiber propagation.[7,25,51] We therefore expect a strong potential for the development of quantum-inspired detection techniques with high sensitivity for fundamental studies in photonics as well as for applications in laser development, multiphoton imaging, and spectroscopy.

METHODS

In order to gain access to incoherent (i.e., nonrepetitive) fluctuations in the spectral domain, the dispersive Fourier transform, illustrated in Figure 1a, constitutes a widely implemented technique. In the case where the dispersive fiber is long enough to ensure a far-field condition[5] (analogous to the Fraunhofer diffraction in the spatial domain[3]), one can sequentially capture time-stretched replicas of the fluctuating spectra in the temporal domain. Using optoelectronic detection, encompassing ultrafast oscilloscopes and detectors, allows extracting successive "spectral" intensity profiles that can be analyzed with standard statistical tools (Figure 1b). The use of spectral correlation maps then allows for getting significant insight into the noise-dependent frequency conversion dynamics during nonlinear propagation.[7] Specifically, these correlation maps can be calculated to find linear dependencies between wavelengths (λ_1, λ_2) using Pearson correlation as defined in eq 1:

$$\rho_{(\lambda_1,\lambda_2)} = \frac{\langle I(\lambda_1)I(\lambda_2)\rangle - \langle I(\lambda_1)\rangle\langle I(\lambda_2)\rangle}{\sqrt{\langle I^2(\lambda_1)\rangle - \langle I(\lambda_1)\rangle^2}\sqrt{\langle I^2(\lambda_2)\rangle - \langle I(\lambda_2)\rangle^2}} \tag{1}$$

Equation 1 allows for constructing the spectral correlation maps retrieved experimentally from DFT-recorded spectral fluctuations $I(\lambda)$ or, alternatively, from an ensemble of Monte Carlo simulations (for which angle brackets represent the average over the ensemble). The coefficient ρ indicates a positive correlation ($0 < \rho \leq 1$) where the intensities of two wavelengths increase or decrease together, an anticorrelation ($-1 \leq \rho < 0$) where the intensity of λ_1 increases when that of λ_2 decreases (and vice versa), and an absence of correlation when $\rho = 0$.

Such correlation maps thus provide detailed statistical information on all of the spectral components' respective links and relationships within the analyzed incoherent spectrum. It allows, in this case, to study how noise impacts the MI dynamics of four wave mixing (FWM) cascaded features and nonlinear broadening signatures. It also has broader applications in identifying important attributes in the fields of nonlinear optics and laser science (such as soliton spectral jitter, pulse collision/trapping, spectrally localized energy depletion, spontaneous or stimulated conversion processes, etc.).[7,13,14,26−28] However, as detailed above, this approach suffers from sensitivity limitations associated with optoelectronic detection, impairing applications requiring

https://doi.org/10.1021/acsphotonics.3c00711
ACS Photonics 2023, 10, 3915−3928

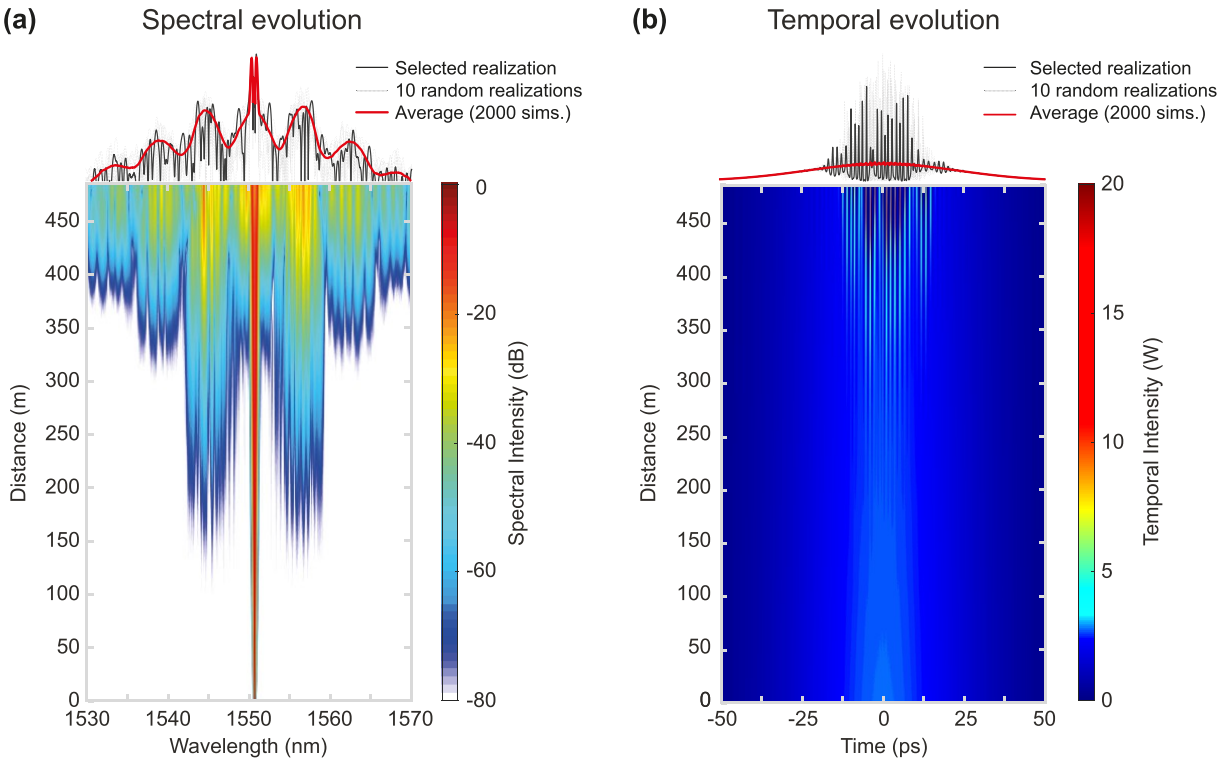

Figure 2. Typical spectral (a) and temporal (b) evolutions of a picosecond pulse experiencing incoherent nonlinear broadening during fiber propagation, here mediated by spontaneous (noise-driven) modulation instability. The numerical results are obtained considering a 55 ps pulse propagating into 485 m of HNLF. The spectral and temporal output displayed in the top panel are obtained from Monte Carlo simulations where each numerical realization is simulated from different noise seeds. The incoherent nature of such noise-driven spectral broadening is shown when comparing the output profiles of ten different realizations (gray lines) with a single (randomly selected) realization (black line) whose propagation dynamics are illustrated in the false color maps. In contrast, the mean output spectrum (red line), averaged from 2000 different realizations, displays an artificially smooth shape as one would observe experimentally from "slow" OSA measurements typically integrating the spectrum from several millions of subsequent optical waveforms.

ultrafast measurements of low-intensity features or the high dynamic range processing of fluctuating optical signals.[6,7,18]

Here, we propose to leverage this DFT technique through ultrasensitive measurements provided by SPDs. With our quantum-inspired DFT approach, each SPD typically detects individual photons every few laser periods while the associated timing module (time-tagger) registers the arrival time of such detected photoevents (i.e., photon-time stamps). Paired with DFT, such a time-resolved SPD detection acts as an ultrasensitive spectrometer, with a time-bin probability of detection directly related to the spectral intensity of the signal under test $I(\lambda)$. In this case, after applying the time-to-frequency mapping of the DFT conversion, the probability of detecting a photon at a wavelength λ_i can be inferred from the analysis of photoevent time-stamps t_k so that, for a total of N detected photons, the probability density distribution P_{λ_i} is given as

$$P_{\lambda_i} \equiv P_{t_i \pm \Delta\tau/2} = \frac{1}{N}\sum_{k=1}^{N} t_k \in \left[t_i - \frac{\Delta\tau}{2};\ t_i + \frac{\Delta\tau}{2}\right] \tag{2}$$

In eq 2, $\Delta\tau$ corresponds to the width of the temporal-bin used in the time-tagger post-processing. t_k is the time-stamp of the photoevent of index k (relative to the laser period t_{laser}) as detected within an integration time spanning numerous laser pulses of indices n_k. The absolute arrival time of a photoevent is given as $t = n_k t_{\text{laser}} + t_k$, which is also impacted by the timing jitter σ_t of the SPD detection, corresponding to the joint temporal jitter[43] of the detectors σ_{SPD} and the time-tagger σ_{TT} yielding $\sigma_t = \sqrt{\sigma_{\text{SPD}}^2 + \sigma_{\text{TT}}^2} = 25$ ps. For a rigorous approach, the timing uncertainty of this detection process can be modeled by convoluting the real probability distribution P_{t_i} with a Gaussian distribution of the standard deviation σ_t. This analysis may then provide the equivalent spectral resolution of our quantum-inspired DFT measurement directly related to the dispersion D_{DFT} of the dispersive fiber (i.e., $\sigma_\lambda = \sigma_t/D_{\text{DFT}}$), as well as a selection of the minimal bin-width $\Delta\tau$ to be used.

Importantly, in contrast to real-time DFT acquisition, SPD-based DFT constitutes a sparse detection where the probability P_{λ_i} is computed from many subsequent spectra n (with an SPD dead time of 60−80 ns ensuring no more than one photoevent detection per laser period). In this context, a single SPD acquisition drastically hampers the ability to conduct meaningful statistical analysis. Exploiting multiple SPDs for DFT measurement can circumvent these issues and thus enable gaining direct access to both the inter- and intrapulse dynamics. This approach is presented in Figure 1c, where we illustrate how the processing of detection events recorded from each SPD allows retrieving the joint probability $P_{\lambda_1,\lambda_2} = P(\lambda_1, \lambda_2) = P(\{\lambda_{\text{SPD1}} = \lambda_1\} \cap \{\lambda_{\text{SPD2}} = \lambda_2\})$ for the coincident detection of a photon at a wavelength λ_1, detected by the first detector (i.e., SPD1) and a photon at a wavelength λ_2, detected by the second detector (i.e., SPD2). In this case, the postselection of the coincidence detection can be made to analyze photoevents originating from the same laser pulse,

https://doi.org/10.1021/acsphotonics.3c00711
ACS Photonics 2023, 10, 3915−3928

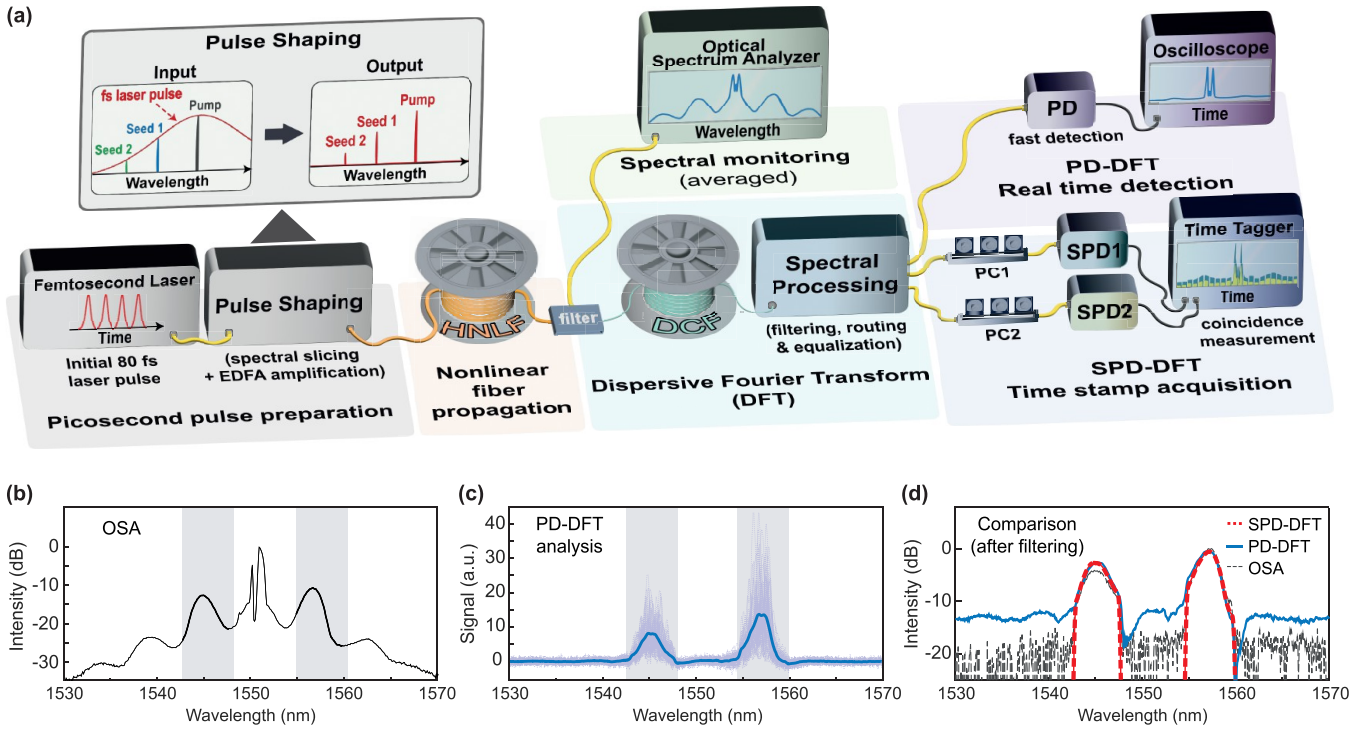

Figure 3. (a) Experimental setup: a femtosecond pulse is spectrally filtered and amplified via an erbium-doped fiber amplifier (EDFA) to generate 55 ps pulses with an adjustable wavelength and phase around 1550 nm. The pulses are then sent into 485 m of highly nonlinear fiber (HNLF) where they experience nonlinear spectral broadening in an anomalous dispersion regime (Figure 2). After HNLF propagation, the broadband incoherent spectrum can be readily monitored by an optical spectrum analyzer (OSA) with long integration time, or the corresponding shot-to-shot spectra can otherwise be measured via dispersive Fourier transform (DFT). In this case, the optical signal at the HNLF output is sent into a dispersion compensating fiber (DCF) after filtering out the pump from the broadband spectrum (to ensure linear propagation in the DCF). After DCF propagation, the time-stretched replica of the spectrum can be captured in the temporal domain with an equivalent resolution of 468 ps/nm (Figure 1a). Such time-stretched spectra can be measured via standard optoelectronic detection (i.e., PD-DFT) encompassing a 6 GHz bandwidth photodiode (PD) and real-time oscilloscope (see Figure 1b) or via quantum-inspired coincidence detection (i.e., SPD-DFT) featuring two single-photon detectors (SPD1 and SPD2) and associated timing electronics (time tagger) for the analysis of detected photoevents with ∼25 ps temporal resolution (see Figure 1c). Prior to detection, we note that the DFT signal can be spectrally processed via a Fourier programmable filter to provide selective filtering (to fully remove the pump or select a region of interest), attenuation (to avoid detector saturation or perform suitable spectral signal equalization) or routing of the signal to the different detectors (with additional polarization controller PC1 and PC2). (b) Broadband output spectrum measured with an OSA with the first MI sidebands highlighted in gray. (c) Output spectrum from PD-DFT based measurements. The DFT analysis shows 500 fluctuating spectra (light dotted lines) along with the computed average spectrum (thick solid blue line) measured after selective filtering of the first MI sidebands (highlighted in gray). (d) Comparison of DFT approaches for the analysis of MI spectral instabilities. The comparison of the filtered OSA (dotted gray), average PD-DFT (solid blue), and average SPD-DFT (dashed red) spectra of the first MI sidebands demonstrates the good agreement of these approaches for a limited dynamic range above the detection noise floor.

designated as intrapulse events (see blue arrows in Figure 1c), where $n_{k,\lambda_1} = n_{k,\lambda_2}$, or photoevents originating from the different laser pulses, designated as interpulse events (see red arrows in Figure 1c), where $n_{k,\lambda_1} \neq n_{k,\lambda_2}$.

It is worth mentioning that wavelength-to-time mapping has already been experimentally demonstrated using DFT techniques paired with dual single-photon detectors to study nonclassical states of light,[43,45,50,52−54] using various experimental configurations including Hong−Ou−Mandel (HOM)[44] and Hanbury-Brown and Twiss (HBT)[46] interferometry. Here, we are interested in qualitatively studying intrinsic intrapulse dynamics and wavelength dependencies arising from complex nonlinear instabilities and cascaded frequency conversion phenomena. In this sense, the study of incoherent spectral fluctuations can be readily pursued by analyzing the different probability features between intrapulse events, interpulse events, and independent detections. In particular, to analyze and gain physical insight into the MI dynamics, here we retrieve intrapulse wavelength dependencies by performing a mutual information analysis (MIA)[55] defined in eq 3:

$$\mu_{(\lambda_1,\lambda_2)} = P_{\lambda_1,\lambda_2} \log\left(\frac{P_{\lambda_1,\lambda_2}}{P_{\lambda_1} P_{\lambda_2}}\right) \tag{3}$$

This statistical tool enables measuring both linear and nonlinear dependencies between two random variables, which was for instance demonstrated to study and underpin elusive parametric processes in laser physics.[26,30] Here, we apply this approach to study the mutual information between incoherent spectral fluctuations to provide a measurement of spectral correlations similar to the Pearson correlation given in eq 1. Importantly, the mutual information metric of eq 3 consists of a relative measurement, thus circumventing statistical bias and measurement uncertainties of eq 2 related to SPD deadtime, quantum efficiency, and their associated wavelength dependency. In this framework, SPD-DFT and MIA are expected to provide ultrasensitive measurements with bias-free statistical analysis of conditional probabilities and

https://doi.org/10.1021/acsphotonics.3c00711
ACS Photonics 2023, 10, 3915−3928

spectral correlations encountered within incoherent nonlinear dynamics (see Supporting Information and Figure S1 for further details on mutual information signal processing).

In this work, we focus on the dynamics occurring when a picosecond pulse propagates through a nonlinear optical fiber within a weakly anomalous dispersion regime (group velocity dispersion parameter $\beta_2 < 0$). This scenario is often encountered in nonlinear fiber optics and constitutes an archetypical example of dynamics involved in incoherent supercontinuum (SC) generation.[56] The pulse evolution is governed by a self-focusing nonlinear Schrödinger equation (NLSE), and the initial spectral broadening is associated with the development of modulation instability.[25] Such propagation dynamics are illustrated in Figure 2, where we display the spectrotemporal evolution of a 55 ps pulse (full width at half-maximum, FWHM) injected within 485 m of highly nonlinear fiber (HNLF) with a peak power P_0 = 2.7 W and a central wavelength of 1550.65 nm. In this case, the pulse propagation is modeled by the generalized nonlinear Schrödinger equation (GNLSE) numerically solved with a split-step Fourier method.[56] For these simulations, we consider realistic experimental conditions (see below) for a propagation into a custom-designed HNLF (Germanium-doped silica fiber) whose dispersion parameters at λ_0 = 1550.65 nm are β_2 = −1.78 $ps^2\,km^{-1}$, β_3 = 0.07 $ps^3\,km^{-1}$ and the nonlinear parameter is γ = 8.4 $W^{-1}\,km^{-1}$.

As seen in Figure 2, the pulse spectral broadening is initiated by noise-driven MI, where the first sidebands appear after ∼120 m of propagation. These sidebands are generated through the exponential amplification of noise located within the MI gain region, symmetrically distributed around the pump. During propagation, the pump also experiences self-phase modulation (SPM),[57] and after ∼310 m within the fiber, one can observe the progressive formation of cascaded four-wave mixing associated with the formation of higher-order MI sidebands (where the MI sidebands generated from noise amplification can in turn act as a pump for FWM conversion).[25,28,58] In the temporal domain, the cascaded MI process leads to highly localized femtosecond structures growing onto the initial picosecond pulse's envelope. This "sea of pulses"[9] corresponds to the onset stage of soliton fission, known to drive incoherent spectral broadening in a weakly anomalous dispersion regime.[56] Shot-to-shot spectral and temporal fluctuations can be readily observed numerically (see gray and black traces in Figure 2) through Monte Carlo simulations using the same parameters but different initial noise seeds. However, these output fluctuations are typically averaged out by long integration times when using experimental characterization techniques such as an optical spectrum analyzer, resulting in the artificially smooth spectral (or temporal) signal intensity shown in Figure 2 (red lines).

To experimentally demonstrate the performance of our approach, we developed the setup illustrated in Figure 3. In this configuration, a 50 MHz mode-locked laser (Menlo Systems, C-fiber) emitted hyperbolic secant pulses centered at 1550.65 nm with a duration of 80 fs (FWHM). These pulses featuring a broadband spectrum were spectrally sliced via a Fourier programmable filter (Finisar, Waveshaper 4000A) using a 15 GHz bandpass filter (FWHM ≈ 0.12 nm). The picosecond pulses obtained after spectral filtering (with peak power from 0.8 to 2 mW) were then amplified through an erbium-doped fiber amplifier (EDFA) at a constant pumping current (880 mA) to reach an average power up to 25 mW. To limit the impact of the intrinsic amplified spontaneous emission (ASE) from the EDFA, the broadband ASE noise was filtered via a bandpass filter with 0.8 nm bandwidth (Newport, TBF-1550-1.0) centered at the pump wavelength before propagation into 485 m of HNLF. In a regime of weak anomalous dispersion, the 55 ps pulses (FWHM) experienced nonlinear spectral broadening driven by SPM and spontaneous MI, so as to follow propagation dynamics similar to those illustrated in Figure 2.

After nonlinear propagation, the broadband, yet incoherent spectrum can be readily monitored via (averaged) OSA measurements. However, to analyze the shot-to-shot spectral fluctuations of the MI spectrum, we perform DFT-based measurements as detailed in Figure 1. For a meaningful comparison between the two DFT approaches, we prepared a broadband signal with a sufficient spectral dynamic range to be readily monitored with both techniques. In this context, we first used a notch filter to eliminate most of the pump from the output MI spectrum before injection into a dispersion-compensating fiber (Figure 3b). This operation allows for ensuring a pure linear propagation in the DCF, so that the spectrum is stretched in the time domain with a dispersive factor of D_{DFT} = 468 ps/nm. In this case, the DFT conversion provides a spectrum, in the time domain, typically spanning 19 ns within a 35 dB bandwidth over the range 1530−1570 nm (Figure 3b).

After temporal stretching, the DFT signal can be directly measured via a fast photodiode and real-time oscilloscope featuring a 6 GHz bandwidth detection (i.e., PD-DFT). Additionally, the signal can be split and captured via superconducting nanowire single-photon detectors (i.e., SPDs). In this case, the incident polarization on each SPD is optimized and the coincidence measurement between the detectors, illustrated in Figure 1c, is performed via photon arrival times retrieved by a start−stop timing electronics unit (Swabian Instruments, time-tagger module). With this approach (i.e., SPD-DFT), the overall temporal jitter associated with time stamp acquisition is 25 ps, which would correspond to an analysis bandwidth of 40 GHz. Both PD- and SPD-based detections are synchronized with the laser emission at 50 MHz, allowing for a straightforward comparison between measurement schemes, which can be readily selected via an additional Fourier programmable filter (Finisar, Waveshaper 4000A/X) placed after the DCF (see Figure 3a,d). Besides allowing for the selective routing of the desired DFT optical signals between detectors with minimal losses (∼6 dB), this waveshaper provides an efficient way of spectrally filtering regions of interest within the output spectrum (see, e.g., Figure 3c,d) or to enable further equalization between the different spectral components of the DFT signal (see Figure 6).

Finally, we note that the first Fourier programmable filter used for the initial pulse shaping can also be leveraged to tailor the picosecond pulse properties before nonlinear propagation. For instance, this approach can be implemented experimentally for adding weak but coherent optical seeds to copropagate with the 55 ps pump pulse into the HNLF. This approach is illustrated in Figure 7, where the impact of the phase from spectrally detuned seeds can be readily observed on the dynamics of noise-driven nonlinear frequency conversion processes.

https://doi.org/10.1021/acsphotonics.3c00711
ACS Photonics 2023, 10, 3915−3928

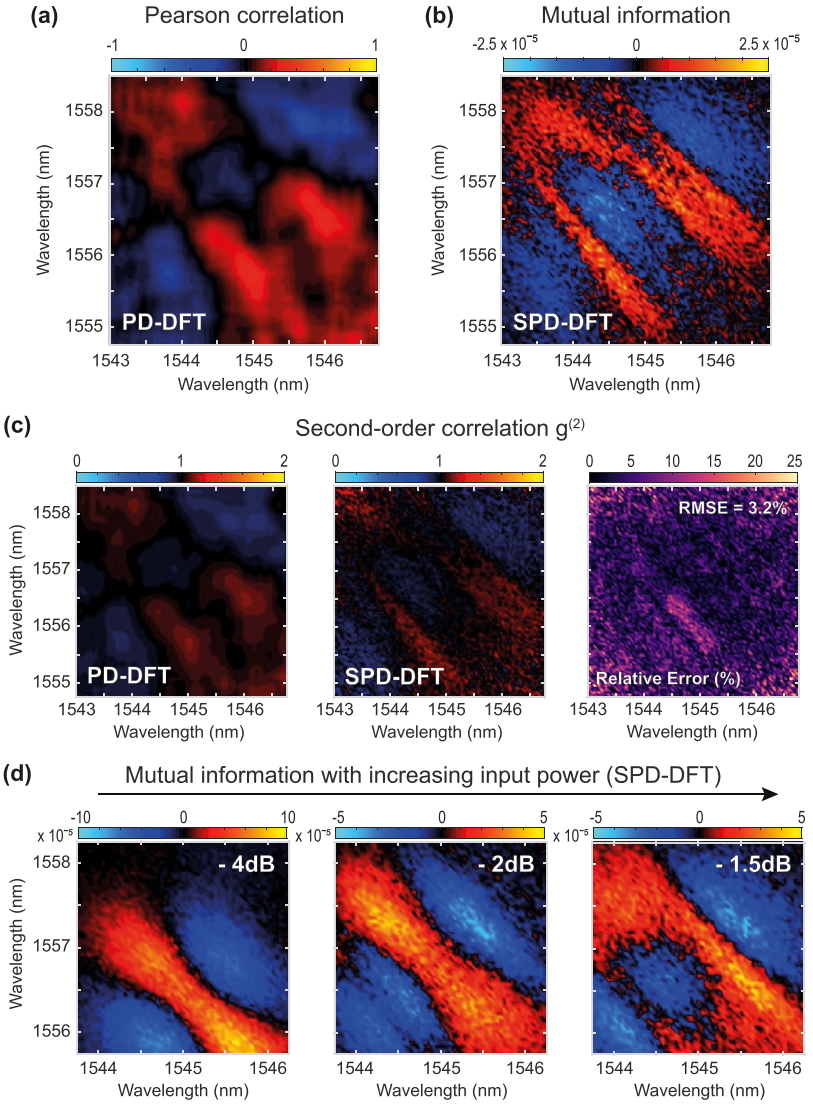

Figure 4. (a) Spectral Pearson correlation map of the first MI sidebands obtained from PD-DFT spectral fluctuation analysis (with 500 shot-to-shot spectral traces captured in 5 min). (b) Spectral mutual information map of the first MI sidebands obtained from SPD-DFT analysis (with 30 min integration time). (c) Corresponding spectral second-order correlation map $g^{(2)}$ obtained from both PD-DFT and SPD-DFT analysis, as well as the relative error computed between each map $g^{(2)}$. (d) Zoom-in of spectral mutual information maps obtained from SPD-DFT analysis for increasing pump power, attesting to the progressive development of more complex correlation structures in the MI sidebands. The power is adjusted by attenuating the pump signal with the waveshaper from −4 to −1.5 dB prior to EDFA amplification and subsequent nonlinear propagation (to maintain the ASE noise constant for each case). The case in panels a−c corresponds to 0 dB attenuation (i.e., ∼8.5 W input peak power pulse), whose output spectra are displayed in Figure 3b−d.

RESULTS AND DISCUSSION

In order to provide a meaningful comparison between these DFT techniques, we first study the fluctuations associated with MI spectral broadening within a limited region of the output spectrum. As illustrated in Figure 3b, when considering only the first MI sidebands symmetrically distributed around the pump (gray shadings), the average spectrum measured with the OSA is contained within a spectral range of ∼13 dB. For these MI sidebands, respectively centered at 1545 and 1557 nm, the corresponding spectral fluctuations can thus be readily captured by exploiting an optimal dynamic range of 8-bit optoelectronic detection schemes without saturation effects (i.e., up to 24 dB for ideal 8 bit digitizers). This feature is illustrated in Figure 3c, where we display the spectral fluctuations of the first MI sidebands measured via our PD-DFT scheme, here obtained after filtering out adjacent spectral components (gray shadings). Importantly, we have verified that after filtering, the average spectrum obtained via PD-DFT measurement exhibits an excellent agreement with both the experimental OSA spectrum and the experimentally measured SPD-DFT spectrum (see Figure 3d).

Analyzing 500 shot-to-shot DFT traces captured with the oscilloscope over 5 min of measurements (see Supporting Information for details), we can perform a statistical analysis of the spectral correlation between the two MI sidebands using the Pearson formula given in eq 1. As illustrated in Figure 4a, the reconstructed correlation map recovered from this 6 GHz detection exhibits well-known features of spontaneous MI processes, where the nonlinear spectral reshaping of the pump by SPM (i.e., symmetric pump modulation and progressive sidelobes formation) can somehow be inferred from the structure of correlations between FWM sidebands.[14,27,57]

https://doi.org/10.1021/acsphotonics.3c00711
ACS Photonics 2023, 10, 3915−3928

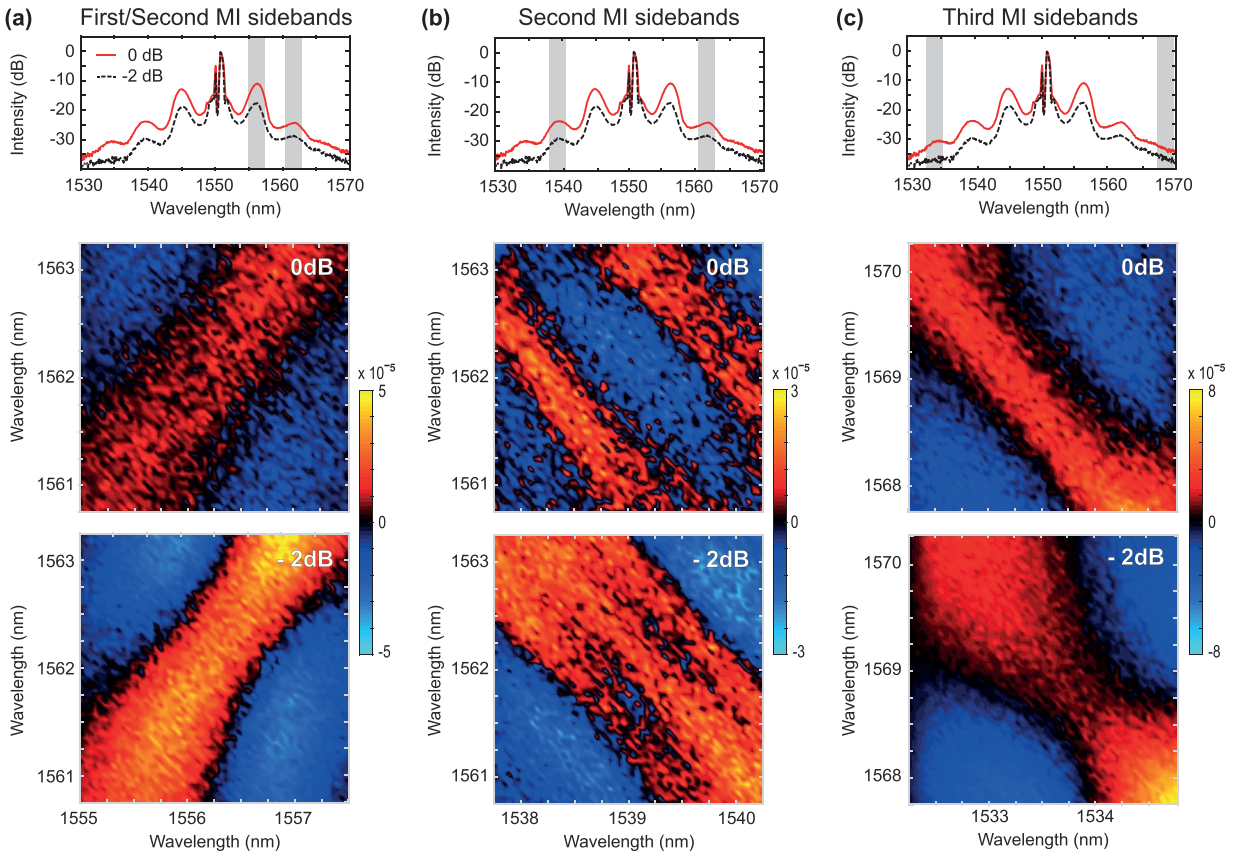

Figure 5. Spectral mutual information maps obtained after HNLF nonlinear broadening for two different input powers. The spectral maps are experimentally measured with SPD-DFT after filtering different MI sidebands to be sent on each SPD (with 30 min integration time). The selected spectral regions of interest are highlighted in the OSA spectra (top panel) and obtained for different input pulse attenuations of 0 dB (red line) and −2 dB (dashed black line). The spectral regions of interest include (a) combination of first and second MI sidebands in the long wavelength edge of the spectrum, (b) second MI symmetrical sidebands, and (c) third MI symmetrical sidebands.

Remarkably, the analogous spectral "mutual information" map retrieved from SPD-DFT measurements show similar features but with a significantly enhanced spectral resolution—reduced from 0.356 nm (for PD-DFT) down to 0.053 nm (for SPD-DFT).

In Figure 4b, we show the result of a mutual information analysis based on eq 3 and performed over 8.5 million coincident photoevent detections between the two independent SPDs obtained after 30 min of measurements (see Supporting Information and Figure S2 for a discussion on the impact of SPD-DFT integration times). In this case, each MI filtered sideband (Stokes/anti-Stokes) was respectively sent onto a separate SPD so that the joint probability P_{λ_1,λ_2} and the independent probabilities P_{λ_1} and P_{λ_2} can be readily computed from eq 2. When observing the mutual information map of Figure 4b, one can clearly notice fine spectral signatures that are not resolved via PD-DFT in Figure 4a.

For the reconstruction of the mutual information map in Figure 4b, the joint probability P_{λ_1,λ_2} was calculated by considering coincident photon detections between the two detectors within selected wavelength bins, while postselecting photoevents originating from the same input laser pulse (i.e., intrapulse events, where $n_{k,\lambda_1} = n_{k,\lambda_2}$). Here, we considered the case that the independent probabilities P_{λ_1} and P_{λ_2} were respectively obtained by computing the marginal of this joint probability distribution $P_{\lambda_1,\lambda_2}(n_{k,\lambda_1} = n_{k,\lambda_2})$. However, we have verified that this approach was bias-free by calculating the joint probability P_{λ_1,λ_2} from the postselection of coincident photoevents originating from different input laser pulses (i.e., interpulse events, where $n_{k,\lambda_1} \neq n_{k,\lambda_2}$). In this case, we found that the corresponding mutual information was essentially null throughout the whole spectral map, thus ensuring the absence of mutual information between pulses (i.e., interpulse laser coherence) or detectors so that $P_{\lambda_1,\lambda_2}(n_{k,\lambda_1} \neq n_{k,\lambda_2}) \sim P_{\lambda_1}P_{\lambda_2}$ (see Supporting Information and Figure S1 for further details).

While aiming at being readily compared to (linear) Pearson spectral correlations, we note that MIA provides a metric similar to the second-order correlation function $g^{(2)}$, commonly used in quantum optics[59] and corresponding to the intensity analogue of the first-order correlation function widely implemented to compute the coherence degree of classical optical signals.[60] Here, the $g^{(2)}$ function can be computed from both SPD- and PD-based DFT measurements so that

$$g^{(2)}_{\text{PD-DFT}}(\lambda_1, \lambda_2) = \frac{\langle I_i(\lambda_1, \lambda_2) I_j(\lambda_1, \lambda_2)\rangle_{i\neq j}}{\langle |I(\lambda_1, \lambda_2)|^2\rangle}$$

$$\text{and } g^{(2)}_{\text{SPD-DFT}}(\lambda_1, \lambda_2) = \frac{P_{\lambda_1,\lambda_2}(n_{k,\lambda_1} = n_{k,\lambda_2})}{P_{\lambda_1,\lambda_2}(n_{k,\lambda_1} \neq n_{k,\lambda_2})} \quad (4)$$

The $g^{(2)}$ measurement results from each case, along with the relative error map between each DFT approach, are displayed in Figure 4c for completeness. This direct comparison between

https://doi.org/10.1021/acsphotonics.3c00711
ACS Photonics 2023, 10, 3915−3928

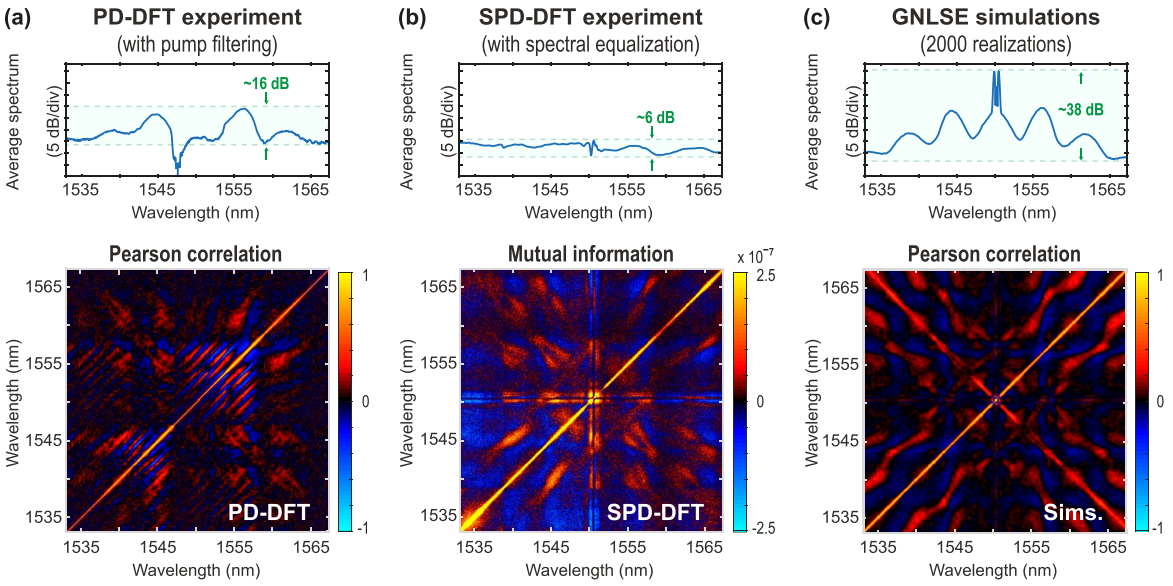

Figure 6. Comparison of the average spectral intensity (top) and the corresponding spectral correlation maps (bottom) retrieved via different approaches for a broadband MI spectrum spanning from 1533 to 1568 nm. (a) Average spectrum and Pearson correlation map retrieved from PD-DFT measurements after pump filtering (to optimize the dynamic range of MI sideband detection) and computed from 500 experimental measurements obtained in 5 min. (b) Average spectrum and mutual information map retrieved from SPD-DFT measurements after spectral signal equalization (with additional attenuation to flatten the average spectrum to its minimal value in the considered spectral range) and 300 min integration time. (c) Average spectrum and Pearson correlation map retrieved from GNLSE simulations with 2000 numerical realizations (ideal case with −120 dB sensitivity cutoff). The green shadings in the average spectra illustrate the dynamic range of the signals considered, in each case, for computing the corresponding correlation maps.

$g^{(2)}$ measurements demonstrates the overall qualitative agreement between the two DFT techniques. The average root-mean-square error (RMSE) between the maps of Figure 4c is 3.2%. Here, this approach is however leveraged to study both linear and nonlinear correlation features between broadband FWM, providing analysis similar to exploring spectral bunching and antibunching within frequency conversion processes. In particular, the use of highly resolved SPD-DFT allows getting access to weakly correlated spectral features where the value of $g^{(2)}$ is close to the case describing coherent light (i.e., $g^{(2)} \sim 1$). Importantly, we here conduct a comparison of PD-DFT and SPD-DFT schemes featuring different temporal resolutions (thus inherently yielding different DFT spectral resolution). However, we note that increasing the PD-DFT detection bandwidth up to 45 GHz to match the speed of our SPD-DFT scheme did not significantly improve the detection efficiency of PD-DFT. In fact, this can eventually degrade the sensitivity, quality, and signal-to-noise ratio (SNR) of the detection and thus hamper the potential reconstruction of spectral correlation maps for the weaker components of the MI spectrum (see Supporting Information and Figures S3 and S4 for a discussion on the impact of PD-DFT detection bandwidth). In this sense, paired with mutual information analysis, our proposed SPD-DFT technique allows gaining additional insights into noise-driven frequency conversion processes of nonlinear physics by means of quantum-inspired measurement techniques, with an improved sensitivity and equivalent spectral resolution out of reach of standard DFT implementations.

To further illustrate this point, we show in Figure 4d the evolution of the spectral map of mutual information within the MI sidebands as a function of the optical pump power. From left to right, one can notice that the increase in the optical power leads to a spectral shift of the MI sideband location as well as a nonlinear reshaping of the pump during pulse propagation in the HNLF (due to the SPM effect). Both features are transposed by FWM and visible in the MI sideband spectral maps of Figure 4d, with a change from a single sideband to the development of more complex correlation signatures (and eventual cascaded FWM processes in the higher-order MI sidebands). These results confirm that SPD-DFT characterization constitutes an important tool for the measurement of complex and nonlinear correlation features within the incoherent broadband signal, here obtained with a spectral resolution similar to standard commercial OSA (i.e., 53 pm with our SPD-DFT technique).

Besides its excellent resolution, a striking feature of this approach arises from the high-sensitivity and low-noise figure provided by the SPDs. PD-DFT measurements are intrinsically limited by their dynamic range and are not able to detect information at low intensities. In contrast, SPD-DFT can overcome such limitations and allow for correlation measurements between weak spectral components. To illustrate this feature, we show in Figure 5 that we could extract mutual information maps between higher-order MI sidebands, resulting in this case from cascaded FWM processes.[13,25,28]

In the mutual information map between the first and second sidebands (Figure 5a), the direct cascaded FWM process between these two adjacent sidebands takes a more prominent role as the power increases but the mutual information map changes marginally. In contrast, in Figure 5b, despite an apparently smooth spectral shape on the OSA, the spectral mutual information maps obtained for the symmetrical second MI sidebands (at 1539 and 1562 nm, respectively) exhibit a clear reshaping when the input pump power increases (in a similar fashion as observed for the first sidebands in Figure 4a). This SPM-like shape is transferred from the pump although there is no direct and trivial FWM process expected to occur

https://doi.org/10.1021/acsphotonics.3c00711
ACS Photonics 2023, 10, 3915−3928

(besides cascaded FWM involving the first sidebands or more complex processes such as e.g. reverse energy flow toward the pump and non-degenerate FWM). Finally, we also can see in Figure 5c that the third MI sidebands located at 1533.5 and 1569 nm can be readily detected. While expected to arise from multiple FWM cascaded conversion, the mutual information reshaping is not so clear: the map remains mostly a diagonal with high values of mutual information associated with the signature of spontaneous processes (whose correlation features are symmetrical on each side of the pump). With this analysis, we demonstrate that the SPD-DFT can provide relevant insight into frequency conversion processes and the statistical distribution of energy occurring between weak spectral components. We note that the analysis is performed at the limit of conventional detection sensitivity (the third MI sideband is at a level as low as −85 dBm, just above the noise floor of the OSA) and with large difference of signal magnitudes (i.e., typically 10 dB intensity difference between sidebands).

An interesting aspect comes from the fact that SPD-DFT theoretically features a dynamic range well above 70 dB (limited only by the count rate saturation of the detectors). As long as the signal is above the noise floor of the SPDs (i.e., approximately −130 dBm), one could integrate photoevents for a sufficiently long time, to accumulate useful coincident detections between all detectable frequency components. However, as two-photon coincidence is a quadratic process, it would thus take an integration time 100 times longer to accumulate the same coincidence counts between spectral components with 10 dB intensity difference compared to signals with the same magnitude (and 10 000 times longer for a 20 dB intensity difference). From an applied viewpoint, this makes such an SPD-DFT approach highly impractical for analyzing broadband spectral fluctuations with a high resolution and a significant dynamic range. Nevertheless, the use of mutual information analysis provides a relative measurement of the correlation between two wavelengths, which is, in fact, independent of the absolute probability of photon detection at a given wavelength (being itself proportional to the spectral intensity to be measured). In this context, we have conducted an experiment to assess the overall agreement and versatility of the two DFT detection schemes over the whole MI spectrum, whose key results are displayed in Figure 6.

For the PD-DFT technique, shot-to-shot spectral fluctuations are recorded from 500 realizations, after filtering out the pump around 1550 nm (in order to resolve the MI sidebands with the best possible dynamic range, i.e., ∼16 dB in the average spectrum). As seen in Figure 6a, the corresponding spectral correlation illustrates MI dynamics with well-defined sideband correlations. However, this statistical analysis is clearly affected by a significant photodiode impulse response (see artifacts in the form of dips in the average DFT spectrum and diagonal correlation stripes in the correlation map) and a limitation of the detection sensitivity observed for higher-order MI sidebands.

For SPD-DFT measurements, we conducted a similar analysis by measuring the whole MI spectrum in each SPD. However, we performed spectral equalization prior to coincidence detection to limit the overall measurement time. Indeed, for demonstrating the robustness of SPD-based detection, we selectively attenuated all spectral components within the MI spectrum. To this end, the average spectrum was measured with the OSA and an opposite attenuation mask was imprinted onto the DFT signal by the waveshaper prior to SPD acquisition. In this case, the spectral intensity is flattened to meet the intensity level of the weakest spectral components in the spectrum (with up to −35 dB attenuation at the pump wavelength). Yet, while the average spectral shape is significantly altered (and its spectral intensity contrast compressed below 6 dB), coincident detections can be readily acquired with SPD-DFT over the whole 35 nm spectral bandwidth of the MI spectrum, without an impulse response nor a sensitivity cutoff. The corresponding mutual information map, retrieved here with an integration time of 300 min (see the Supporting Information), is thus obtained for the whole MI spectrum without visible limitation of the dynamic range nor the appearance of measurement artifacts.

Noteworthy, spectral equalization is not possible for the PD-DFT technique, for which the signal would fall below the detection noise floor (see, for instance, the comparison of the average spectral intensity level between Figure 6a,b, as well as the Supporting Information). Moreover, it is worth noting that this SPD-DFT technique allows for improving the signal quality through prior knowledge of the measurement process. For instance, we expect the mutual information maps to be symmetric along its diagonal so that $\mu_{(\lambda_1,\lambda_2)} = \mu_{(\lambda_2,\lambda_1)}$. Through our SPD-DFT measurements over the full spectrum acquired by both SPDs, we can directly retrieve a compound (symmetric) value of this mutual information map, as displayed in Figure 6b, in order to further reduce the measurement noise and statistical bias of our analysis.

The mutual information, although yielding a slightly different metric than Pearson correlation, provides a clear map of the frequency conversion dynamics in good qualitative agreement with the numerical results displayed in Figure 6c. In this case, the Pearson correlation map is computed using GNLSE simulations to generate 2000 Monte Carlo realizations (from random input noise). While the contrast is different, it appears clearly that SPD-DFT measurements along with refined mutual information analysis provide an important tool for identifying key dynamics and analyzing spectral fluctuations with good fidelity.

To further investigate the performance of our new approach, we experimentally studied more complex frequency conversion processes associated with modulation instability. In this case, we considered a scenario where spontaneous MI (i.e., noise-driven) is competing with induced MI, arising from a weak modulation on the initial optical wave. To do so, we consider the same optical setup but with the addition of two weak and coherent optical seeds that copropagate with the pump signal in the HNLF (see Methods and Figure 3a). Specifically, we added two picosecond pulse seeds to the input signal by directly filtering the initial femtosecond pulse via the waveshaper, using the same spectral "slicing" process on the broadband laser spectrum as the one used to generate the picosecond pump pulse (i.e., a 15 GHz bandpass filtering). As a result, the seeds are in this case coherent (same laser source), with the same 55 ps duration (same filtering process) and temporally overlapped (same optical path) until reaching the HNLF. However, the two optical seeds present significantly lower power than the pump (less than 0.16%) as obtained by the additional 28 dB attenuation set on the waveshaper filtering. It is worth noting that the seed spectral intensities are at a level comparable to the ASE noise of the EDFA, so that

https://doi.org/10.1021/acsphotonics.3c00711
ACS Photonics 2023, 10, 3915−3928

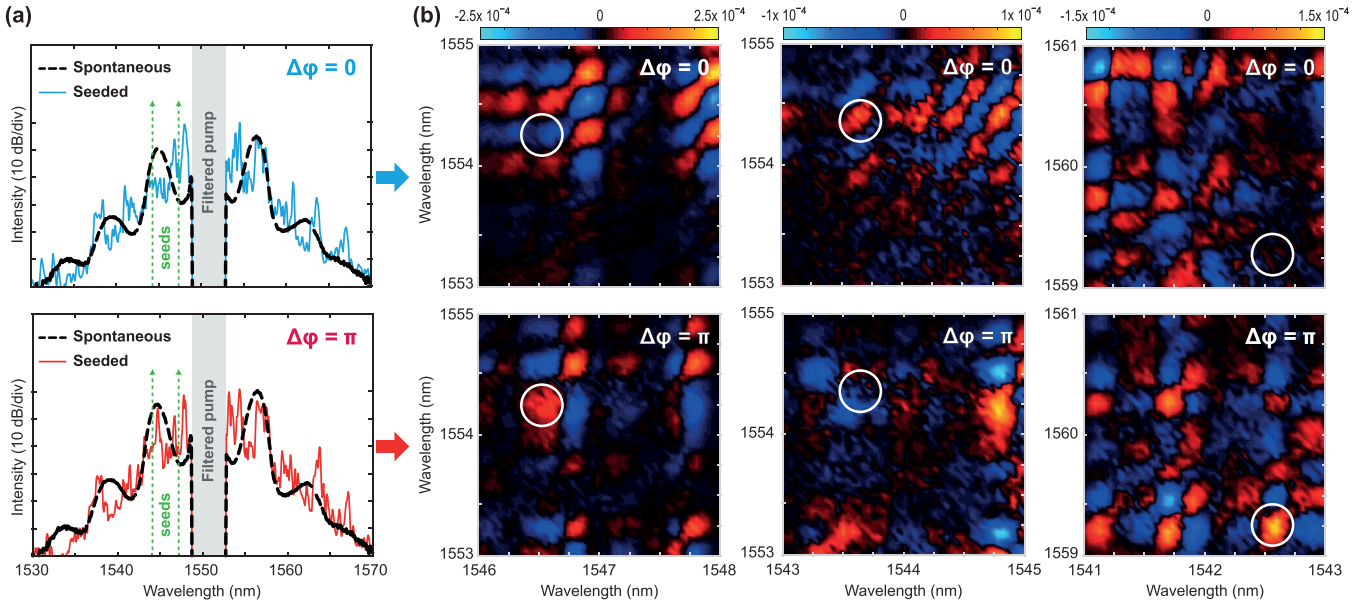

Figure 7. (a) Output MI spectra obtained by the addition of two coherent input seeds at a frequency detuning of 400 and 800 GHz respectively (green arrows), with different spectral phase difference $\Delta_\phi = 0$ (blue) and $\Delta_\phi = \pi$ (red). The MI seeded spectra are compared with the spontaneous MI spectrum (black dashes) for clarity. (b) Corresponding spectral mutual information maps experimentally measured with SPD-DFT (30 min integration time) after filtering different regions of the MI output spectrum when the input pump pulse copropagates in the HNLF with two weak coherent seeds. One can see that the sign (and shape) of the mutual information map can be effectively manipulated by the addition of weak input coherent seeds with opposite phases, as highlighted in the white circled areas of the maps.

the induced and spontaneous MI processes are in direct competition.

Importantly, such a coherent spectral processing allows for readily controlling the detuning and phase of the seeds compared to the pump pulse. For instance, for the results presented in Figure 7, we considered the case where the two seeds are respectively detuned from the pump by Δf_1 = 400 GHz and Δf_2 = 800 GHz, corresponding to seed wavelengths at 1547.4 and 1544.3 nm. This configuration, where both seeds are located within the MI gain region and feature harmonic detuning where $\Delta f_2 = 2\Delta f_1$, hints at complex degenerate and cascaded FWM processes, further competing with noise-driven MI dynamics. We thus studied two specific cases by adjusting the relative spectral phase between the seeds so that $\Delta\phi = 2\phi_0 + \phi_1 + \phi_2$. The results of the SPD-DFT measurements are shown in Figure 7, for two nonlinear propagation scenarios where $\phi_1 = \phi_2 = 0 \Rightarrow \Delta\phi = 0$ and $\phi_1 = 0$, $\phi_2 = \pi \Rightarrow \Delta\phi = \pi$, respectively. By extracting the mutual information for different MI sideband combinations (Figure 7b), we can readily see that the optical seeding significantly impacts the MI broadening dynamics and the corresponding spectral maps obtained after nonlinear propagation. Even for such incoherent output spectra, the extremely weak input modulation can drastically reshape the frequency conversion dynamics and the associated mutual information on the wavelengths closest to the pump (1547 and 1554 nm) up to further spectrally detuned frequency components arising from cascaded FWM processes (1542 and 1560 nm). In fact, for all MI sideband combinations displayed in Figure 7, we can see that a change in the phase of the optical seeds can alter both the layout and sign of the mutual information map at specific wavelengths (see the white-circled area in the maps). While not unexpected from a theoretical viewpoint, these results illustrate the power of SPD-DFT and mutual information analysis for gaining insight into both complex incoherent dynamics and cascaded frequency conversion processes that are difficult to assess using more conventional methods.

CONCLUSIONS

We have experimentally demonstrated a quantum-inspired approach for the spectral characterization of incoherent photonics processes. Leveraging the dispersive Fourier transform, a well-known concept borrowed from classical fiber optics, we have demonstrated the ability to perform spectral correlation measurements among broadband and fluctuating optical signals by means of coincident photoevents acquired by single-photon detectors. While such a sparse detection may not provide access to real-time measurements of shot-to-shot spectral fluctuations, SPD-DFT and mutual information analysis can yield similar spectral signatures and statistical features as standard DFT analysis (or other conventional detection methods). Remarkably, the low temporal jitter and excellent quantum efficiency provided by SPDs allowed us to demonstrate a novel DFT approach with significantly better performances in terms of signal sensitivity, spectral resolution, and measurable dynamic range. Here, we demonstrated a DFT implementation allowing the measurement of incoherent spectral features with a resolution of ∼53 pm, which proved useful to measure high dynamic range and very low intensity signals that can merely be resolved by an averaged optical spectral analyzer (and out of the reach of standard real-time characterization techniques).

Within this study, we specifically showed that this innovative DFT approach can be leveraged to analyze modulation instability, an archetypical nonlinear process commonly encountered in guided optics. Our SPD-DFT implementation allowed for readily analyzing statistical relationships and correlations between extremely weak spectral components. For instance, noise-driven MI dynamics and their incoherent cascaded FWM processes have been successfully characterized

https://doi.org/10.1021/acsphotonics.3c00711
ACS Photonics 2023, 10, 3915−3928

up to the third sideband with a sensitivity level well-above standard DFT implementation and without the emergence of visible measurement artifacts otherwise arising from ultrafast photodiode impulse responses. It is noteworthy that we have shown that spectral mutual information analysis allowed for identifying subtle changes in the correlation features of the output spectrum when adjusting slightly the initial conditions. The competition between noise-driven (spontaneous) and coherently seeded (induced) MI dynamics can be experimentally identified within all spectral sidebands. In this framework, by merely adjusting the phase of weak input optical seeds, we demonstrated the potential for tailoring the shape of the spectral mutual information maps (and fine-tuning the correlations between specific wavelengths) after nonlinear broadening.

From a fundamental viewpoint, we foresee our results as paving the way toward tailoring specifically tuned nonlinear interactions in fiber optics, thus enabling further control of noise-driven processes at the boundary between quantum and nonlinear optics. In particular, in the low-power regime readily monitored with SPD-DFT, we anticipate important impacts in the framework of advanced all-optical signal processing with applications spanning phase-sensitive amplification and the control of quantum states. From a practical aspect, we expect that our quantum-inspired DFT characterization may prove useful for the acquisition of broadband signals (e.g., supercontinuum) in applications requiring the monitoring of incoherent signals with high dynamic range (as typically required for the deployment of machine-learning strategies in ultrafast photonics). Similarly, we anticipate that such a DFT technique will have strong potential for imaging and microscopy applications requiring both high sensitivity and advanced spectral detection. In particular, computational imaging, correlated microscopy, and multiphoton spectroscopy may directly benefit from this SPD-DFT tool when performing nonrepetitive multidimensional signal analysis.

Finally, on a more technical note, we want to highlight that our proof-of-principle demonstration allowed for the measurement of a 40 nm bandwidth spectrum with excellent resolution and with an optimized integration time thanks to broadband signal equalization. The ability to perform such a measurement without noticeable limitation in the power spectral (temporal) density of the DFT signal is significant (Supporting Information). This hints toward the potential of further DFT temporal stretching of the optical spectrum, which was here limited by the laser repetition rate and available dispersive fiber module. However, we expect that advanced DFT processing[5−7] such as pulse picking and recirculating fiber loop should be capable of yielding extreme DFT broadening, thus pushing forward the limits of achievable DFT spectral resolution toward the picometer range while, conversely, alleviating the need for expensive low-jitter SPD detection schemes for setups with demanding sensitivity needs but less stringent resolution requirements.

■ ASSOCIATED CONTENT

Supporting Information

The Supporting Information is available free of charge at https://pubs.acs.org/doi/10.1021/acsphotonics.3c00711.

Statistical analysis of inter- and intrapulse dynamics using multiple SPD detection; comparison of measurement times and resolution in SPD-DFT and PD-DFT detection; discussion on spectral resolution and performance improvements using higher detection bandwidth (PDF)

■ AUTHOR INFORMATION

Corresponding Authors

Michael Kues − *Institute of Photonics and Cluster of Excellence PhoenixD, Leibniz University Hannover, 30167 Hannover, Germany*; Email: michael.kues@iop.uni-hannover.de

Benjamin Wetzel − *Xlim Research Institute, CNRS UMR 7252, Université de Limoges, 87060 Limoges, France*; orcid.org/0000-0002-2691-0307; Email: benjamin.wetzel@xlim.fr

Authors

Lynn Sader − *Xlim Research Institute, CNRS UMR 7252, Université de Limoges, 87060 Limoges, France*; orcid.org/0000-0003-2604-1831

Surajit Bose − *Institute of Photonics and Cluster of Excellence PhoenixD, Leibniz University Hannover, 30167 Hannover, Germany*

Anahita Khodadad Kashi − *Institute of Photonics and Cluster of Excellence PhoenixD, Leibniz University Hannover, 30167 Hannover, Germany*

Yassin Boussafa − *Xlim Research Institute, CNRS UMR 7252, Université de Limoges, 87060 Limoges, France*

Raktim Haldar − *Institute of Photonics and Cluster of Excellence PhoenixD, Leibniz University Hannover, 30167 Hannover, Germany*

Romain Dauliat − *Xlim Research Institute, CNRS UMR 7252, Université de Limoges, 87060 Limoges, France*

Philippe Roy − *Xlim Research Institute, CNRS UMR 7252, Université de Limoges, 87060 Limoges, France*

Marc Fabert − *Xlim Research Institute, CNRS UMR 7252, Université de Limoges, 87060 Limoges, France*

Alessandro Tonello − *Xlim Research Institute, CNRS UMR 7252, Université de Limoges, 87060 Limoges, France*

Vincent Couderc − *Xlim Research Institute, CNRS UMR 7252, Université de Limoges, 87060 Limoges, France*

Complete contact information is available at: https://pubs.acs.org/10.1021/acsphotonics.3c00711

Notes

The authors declare no competing financial interest.

■ ACKNOWLEDGMENTS

This work has received funding from the European Research Council (ERC) under the European Union's Horizon 2020 research and innovation programme under grant agreement No. 950618 (STREAMLINE project) and No. 947603 (QFreC project), from the French Agence Nationale de la Recherche (ANR) through the OPTIMAL project (ANR-20-CE30-0004), from the German Federal Ministry of Education and Research within the project PQuMAL and the Deutsche Forschungsgemeinschaft (DFG, German Research Foundation) under Germany's Excellence Strategy within the Cluster of Excellence PhoenixD (EXC 2122, Project ID 390833453). L.S., Y.B., and B.W. further acknowledge the support of the Conseil Régional Nouvelle-Aquitaine (SCIR & SPINAL projects). R.H. acknowledges the financial support provided

by the Alexander von Humboldt Stiftung to conduct the research.

REFERENCES

(1) LIGO Scientific Collaboration and Virgo Collaboration; Abbott, B. P.; et al. Observation of Gravitational Waves from a Binary Black Hole Merger. *Phys. Rev. Lett.* **2016**, *116* (6), No. 061102.
(2) Pohl, R.; Antognini, A.; Nez, F.; Amaro, F. D.; Biraben, F.; Cardoso, J. M. R.; Covita, D. S.; Dax, A.; Dhawan, S.; Fernandes, L. M. P.; Giesen, A.; Graf, T.; Hänsch, T. W.; Indelicato, P.; Julien, L.; Kao, C.-Y.; Knowles, P.; Le Bigot, E.-O.; Liu, Y.-W.; Lopes, J. A. M.; Ludhova, L.; Monteiro, C. M. B.; Mulhauser, F.; Nebel, T.; Rabinowitz, P.; dos Santos, J. M. F.; Schaller, L. A.; Schuhmann, K.; Schwob, C.; Taqqu, D.; Veloso, J. F. C. A.; Kottmann, F. The Size of the Proton. *Nature* **2010**, *466* (7303), 213−216.
(3) Kolner, B. H. Space-Time Duality and the Theory of Temporal Imaging. *IEEE J. Quantum Electron.* **1994**, *30* (8), 1951−1963.
(4) Bhushan, A. S.; Coppinger, F.; Jalali, B. Time-Stretched Analogue-to-Digital Conversion. *Electron. Lett.* **1998**, *34* (9), 839−841.
(5) Zhou, Y.; Chan, J. C. K.; Jalali, B. A Unified Framework for Photonic Time-Stretch Systems. *Laser & Photonics Reviews* **2022**, *16* (8), 2100524.
(6) Mahjoubfar, A.; Churkin, D. V.; Barland, S.; Broderick, N.; Turitsyn, S. K.; Jalali, B. Time Stretch and Its Applications. *Nature Photon* **2017**, *11* (6), 341−351.
(7) Godin, T.; Sader, L.; Khodadad Kashi, A.; Hanzard, P.-H.; Hideur, A.; Moss, D. J.; Morandotti, R.; Genty, G.; Dudley, J. M.; Pasquazi, A.; Kues, M.; Wetzel, B. Recent Advances on Time-Stretch Dispersive Fourier Transform and Its Applications. *Advances in Physics: X* **2022**, *7* (1), No. 2067487.
(8) Foster, M. A.; Salem, R.; Geraghty, D. F.; Turner-Foster, A. C.; Lipson, M.; Gaeta, A. L. Silicon-Chip-Based Ultrafast Optical Oscilloscope. *Nature* **2008**, *456* (7218), 81−84.
(9) Närhi, M.; Wetzel, B.; Billet, C.; Toenger, S.; Sylvestre, T.; Merolla, J.-M.; Morandotti, R.; Dias, F.; Genty, G.; Dudley, J. M. Real-Time Measurements of Spontaneous Breathers and Rogue Wave Events in Optical Fibre Modulation Instability. *Nat. Commun.* **2016**, *7* (1), 13675.
(10) Jannson, T. Real-Time Fourier Transformation in Dispersive Optical Fibers. *Opt. Lett.* **1983**, *8* (4), 232−234.
(11) Tong, Y. C.; Chan, L. Y.; Tsang, H. K. Fibre Dispersion or Pulse Spectrum Measurement Using a Sampling Oscilloscope. *Electron. Lett.* **1997**, *33* (11), 983−985.
(12) Muriel, M. A.; Azaña, J.; Carballar, A. Real-Time Fourier Transformer Based on Fiber Gratings. *Opt. Lett.* **1999**, *24* (1), 1−3.
(13) Solli, D. R.; Herink, G.; Jalali, B.; Ropers, C. Fluctuations and Correlations in Modulation Instability. *Nature Photon* **2012**, *6* (7), 463−468.
(14) Wetzel, B.; Stefani, A.; Larger, L.; Lacourt, P. A.; Merolla, J. M.; Sylvestre, T.; Kudlinski, A.; Mussot, A.; Genty, G.; Dias, F.; Dudley, J. M. Real-Time Full Bandwidth Measurement of Spectral Noise in Supercontinuum Generation. *Sci. Rep.* **2012**, *2*, 882.
(15) Herink, G.; Kurtz, F.; Jalali, B.; Solli, D. R.; Ropers, C. Real-Time Spectral Interferometry Probes the Internal Dynamics of Femtosecond Soliton Molecules. *Science* **2017**, *356* (6333), 50−54.
(16) Chernysheva, M.; Sugavanam, S.; Turitsyn, S. Real-Time Observation of the Optical Sagnac Effect in Ultrafast Bidirectional Fibre Lasers. *APL Photonics* **2020**, *5* (1), No. 016104.
(17) Genty, G.; Salmela, L.; Dudley, J. M.; Brunner, D.; Kokhanovskiy, A.; Kobtsev, S.; Turitsyn, S. K. Machine Learning and Applications in Ultrafast Photonics. *Nat. Photonics* **2021**, *15* (2), 91−101.
(18) Närhi, M.; Salmela, L.; Toivonen, J.; Billet, C.; Dudley, J. M.; Genty, G. Machine Learning Analysis of Extreme Events in Optical Fibre Modulation Instability. *Nat. Commun.* **2018**, *9* (1), 4923.
(19) Weiner, A. M. *Ultrafast Optics*; Wiley series in pure and applied optics; Wiley: Hoboken, N.J, 2009.
(20) Trebino, R. *Frequency-Resolved Optical Gating: The Measurement of Ultrashort Laser Pulses*; Springer US: Boston, MA, 2000. DOI: 10.1007/978-1-4615-1181-6.
(21) Walmsley, I. A.; Dorrer, C. Characterization of Ultrashort Electromagnetic Pulses. *Adv. Opt. Photon.* **2009**, *1* (2), 308−437.
(22) Messager, V.; Louradour, F.; Froehly, C.; Barthelemy, A. Coherent Measurement of Short Laser Pulses Based on Spectral Interferometry Resolved in Time. *Opt. Lett.* **2003**, *28* (9), 743−745.
(23) Pasquazi, A.; Peccianti, M.; Park, Y.; Little, B. E.; Chu, S. T.; Morandotti, R.; Azaña, J.; Moss, D. J. Sub-Picosecond Phase-Sensitive Optical Pulse Characterization on a Chip. *Nat. Photonics* **2011**, *5* (10), 618−623.
(24) Konatham, S. R.; de Chatellus, H. G.; Azaña, J. Photonics-Based Real-Time Spectrogram Analysis of Broadband Waveforms. *Journal of Lightwave Technology* **2020**, *38* (19), 5356−5367.
(25) Dudley, J. M.; Dias, F.; Erkintalo, M.; Genty, G. Instabilities, Breathers and Rogue Waves in Optics. *Nature Photon* **2014**, *8* (10), 755−764.
(26) Touil, M.; Becheker, R.; Godin, T.; Hideur, A. Spectral Correlations in a Fiber-Optical Parametric Oscillator. *Phys. Rev. A* **2021**, *103* (4), No. 043503.
(27) Godin, T.; Wetzel, B.; Sylvestre, T.; Larger, L.; Kudlinski, A.; Mussot, A.; Salem, A. B.; Zghal, M.; Genty, G.; Dias, F.; Dudley, J. M. Real Time Noise and Wavelength Correlations in Octave-Spanning Supercontinuum Generation. *Opt. Express* **2013**, *21* (15), 18452−18460.
(28) Wang, X.; Bigourd, D.; Kudlinski, A.; Wong, K. K. Y.; Douay, M.; Bigot, L.; Lerouge, A.; Quiquempois, Y.; Mussot, A. Correlation between Multiple Modulation Instability Side Lobes in Dispersion Oscillating Fiber. *Opt. Lett.* **2014**, *39* (7), 1881−1884.
(29) Robert, P.; Fourcade-Dutin, C.; Fourcade-Dutin, C.; Dauliat, R.; Jamier, R.; Muñoz-Marco, H.; Pérez-Millán, P.; Dudley, J. M.; Roy, P.; Maillotte, H.; Bigourd, D.; Bigourd, D. Spectral Correlation of Four-Wave Mixing Generated in a Photonic Crystal Fiber Pumped by a Chirped Pulse. *Opt. Lett.* **2020**, *45* (15), 4148−4151.
(30) Sugavanam, S.; Sorokina, M.; Churkin, D. V. Spectral Correlations in a Random Distributed Feedback Fibre Laser. *Nat. Commun.* **2017**, *8* (1), 15514.
(31) Ryczkowski, P.; Närhi, M.; Billet, C.; Merolla, J.-M.; Genty, G.; Dudley, J. M. Real-Time Full-Field Characterization of Transient Dissipative Soliton Dynamics in a Mode-Locked Laser. *Nat. Photonics* **2018**, *12* (4), 221−227.
(32) Lapre, C.; Billet, C.; Meng, F.; Ryczkowski, P.; Sylvestre, T.; Finot, C.; Genty, G.; Dudley, J. M. Real-Time Characterization of Spectral Instabilities in a Mode-Locked Fibre Laser Exhibiting Soliton-Similariton Dynamics. *Sci. Rep* **2019**, *9* (1), 13950.
(33) Bessin, F.; Copie, F.; Conforti, M.; Kudlinski, A.; Mussot, A.; Trillo, S. Real-Time Characterization of Period-Doubling Dynamics in Uniform and Dispersion Oscillating Fiber Ring Cavities. *Phys. Rev. X* **2019**, *9* (4), No. 041030.
(34) Meng, F.; Lapre, C.; Billet, C.; Sylvestre, T.; Merolla, J.-M.; Finot, C.; Turitsyn, S. K.; Genty, G.; Dudley, J. M. Intracavity Incoherent Supercontinuum Dynamics and Rogue Waves in a Broadband Dissipative Soliton Laser. *Nat. Commun.* **2021**, *12* (1), 5567.
(35) Solli, D. R.; Chou, J.; Jalali, B. Amplified Wavelength−Time Transformation for Real-Time Spectroscopy. *Nature Photon* **2008**, *2* (1), 48−51.
(36) Goda, K.; Tsia, K. K.; Jalali, B. Serial Time-Encoded Amplified Imaging for Real-Time Observation of Fast Dynamic Phenomena. *Nature* **2009**, *458* (7242), 1145−1149.
(37) Mahjoubfar, A.; Goda, K.; Ayazi, A.; Fard, A.; Kim, S. H.; Jalali, B. High-Speed Nanometer-Resolved Imaging Vibrometer and Velocimeter. *Appl. Phys. Lett.* **2011**, *98* (10), 101107.
(38) Hanzard, P.-H.; Godin, T.; Idlahcen, S.; Rozé, C.; Hideur, A. Real-Time Tracking of Single Shockwaves via Amplified Time-Stretch Imaging. *Appl. Phys. Lett.* **2018**, *112* (16), 161106.
(39) Mahmudlu, H.; Johanning, R.; van Rees, A.; Khodadad Kashi, A.; Epping, J. P.; Haldar, R.; Boller, K.-J.; Kues, M. Fully On-Chip

Photonic Turnkey Quantum Source for Entangled Qubit/Qudit State Generation. *Nat. Photonics* **2023**, *17*, 518.
(40) Sugavanam, S.; Kopae, M. K.; Peng, J.; Prilepsky, J. E.; Turitsyn, S. K. Analysis of Laser Radiation Using the Nonlinear Fourier Transform. *Nat. Commun.* **2019**, *10* (1), 5663.
(41) Tikan, A.; Bielawski, S.; Szwaj, C.; Randoux, S.; Suret, P. Single-Shot Measurement of Phase and Amplitude by Using a Heterodyne Time-Lens System and Ultrafast Digital Time-Holography. *Nature Photon* **2018**, *12* (4), 228−234.
(42) Naveau, C.; Vanderhaegen, G.; Szriftgiser, P.; Martinelli, G.; Droques, M.; Kudlinski, A.; Conforti, M.; Trillo, S.; Akhmediev, N.; Mussot, A. Heterodyne Optical Time Domain Reflectometer Combined With Active Loss Compensation: A Practical Tool for Investigating Fermi Pasta Ulam Recurrence Process and Breathers Dynamics in Optical Fibers. *Front. Phys.* **2021**, *9*, 637812.
(43) Eckstein, A.; Boucher, G.; Lemaître, A.; Filloux, P.; Favero, I.; Leo, G.; Sipe, J. E.; Liscidini, M.; Ducci, S. High-Resolution Spectral Characterization of Two Photon States via Classical Measurements. *Laser & Photonics Reviews* **2014**, *8* (5), L76−L80.
(44) Gerrits, T.; Marsili, F.; Verma, V. B.; Shalm, L. K.; Shaw, M.; Mirin, R. P.; Nam, S. W. Spectral Correlation Measurements at the Hong-Ou-Mandel Interference Dip. *Phys. Rev. A* **2015**, *91* (1), No. 013830.
(45) Karpiński, M.; Jachura, M.; Wright, L. J.; Smith, B. J. Bandwidth Manipulation of Quantum Light by an Electro-Optic Time Lens. *Nature Photon* **2017**, *11* (1), 53−57.
(46) Khodadad Kashi, A.; Sader, L.; Haldar, R.; Wetzel, B.; Kues, M. Frequency-to-Time Mapping Technique for Direct Spectral Characterization of Biphoton States From Pulsed Spontaneous Parametric Processes. *Front. Photon.* **2022**, *3*, No. 834065.
(47) Crockett, B.; van Howe, J.; Montaut, N.; Morandotti, R.; Azaña, J. High-Resolution Time-Correlated Single-Photon Counting Using Electro-Optic Sampling. *Laser & Photonics Reviews* **2022**, *16* (10), 2100635.
(48) Kolenderska, S. M.; Vanholsbeeck, F.; Kolenderski, P. Quantum-Inspired Detection for Spectral Domain Optical Coherence Tomography. *Opt. Lett.* **2020**, *45* (13), 3443−3446.
(49) Tiedeck, S.; Heindl, M. B.; Kramlinger, P.; Naas, J.; Brütting, F.; Kirkwood, N.; Mulvaney, P.; Herink, G. Single-Pixel Fluorescence Spectroscopy Using Near-Field Dispersion for Single-Photon Counting and Single-Shot Acquisition. *ACS Photonics* **2022**, *9* (9), 2931−2937.
(50) Avenhaus, M.; Eckstein, A.; Mosley, P. J.; Silberhorn, C. Fiber-Assisted Single-Photon Spectrograph. *Opt. Lett.* **2009**, *34* (18), 2873−2875.
(51) Wetzel, B.; Kues, M.; Roztocki, P.; Reimer, C.; Godin, P.-L.; Rowley, M.; Little, B. E.; Chu, S. T.; Viktorov, E. A.; Moss, D. J.; Pasquazi, A.; Peccianti, M.; Morandotti, R. Customizing Supercontinuum Generation via On-Chip Adaptive Temporal Pulse-Splitting. *Nat. Commun.* **2018**, *9* (1), 1−10.
(52) Gerrits, T.; Stevens, M. J.; Baek, B.; Calkins, B.; Lita, A.; Glancy, S.; Knill, E.; Nam, S. W.; Mirin, R. P.; Hadfield, R. H.; Bennink, R. S.; Grice, W. P.; Dorenbos, S.; Zijlstra, T.; Klapwijk, T.; Zwiller, V. Generation of Degenerate, Factorizable, Pulsed Squeezed Light at Telecom Wavelengths. *Opt. Express* **2011**, *19* (24), 24434.
(53) Zielnicki, K.; Garay-Palmett, K.; Cruz-Delgado, D.; Cruz-Ramirez, H.; O'Boyle, M. F.; Fang, B.; Lorenz, V. O.; U'Ren, A. B.; Kwiat, P. G. Joint Spectral Characterization of Photon-Pair Sources. *Journal of Modern Optics* **2018**, *65* (10), 1141−1160.
(54) Francesconi, S.; Baboux, F.; Raymond, A.; Fabre, N.; Boucher, G.; Lemaître, A.; Milman, P.; Amanti, M. I.; Ducci, S. Engineering Two-Photon Wavefunction and Exchange Statistics in a Semiconductor Chip. *Optica* **2020**, *7* (4), 316−322.
(55) Shannon, C. E. A Mathematical Theory of Communication. *Bell System Technical Journal* **1948**, *27* (3), 379−423.
(56) Dudley, J. M.; Taylor, J. R. *Supercontinuum Generation in Optical Fibers*; Cambridge University Press, 2010.
(57) Agrawal, G. P. Nonlinear Fiber Optics. *Nonlinear Science at the Dawn of the 21st Century* **2000**, *542*, 195−211.
(58) Perego, A. M.; Bessin, F.; Mussot, A. Complexity of Modulation Instability. *Phys. Rev. Research* **2022**, *4* (2), No. L022057.
(59) Grynberg, G.; Aspect, A.; Fabre, C.; Cohen-Tannoudji, C. *Introduction to Quantum Optics: From the Semi-classical Approach to Quantized Light*; Cambridge University Press: Cambridge, UK, 2010.
(60) Genty, G.; Surakka, M.; Turunen, J.; Friberg, A. T. Complete Characterization of Supercontinuum Coherence. *J. Opt. Soc. Am. B, JOSAB* **2011**, *28* (9), 2301−2309.

https://doi.org/10.1021/acsphotonics.3c00711
ACS Photonics 2023, 10, 3915−3928